This study investigates the impact of different burning temperatures on quicklime slaking reactivity. Moreover, it reviews the state of the art of the effect of carbonate rock fabrics and calcination kinetics on the production of quicklime in industrial kilns. The burnability and overburning tendency of raw materials with different geological origin, stratigraphic positions, fabrics and compositions were investigated. Burning trials were performed on crushed rocks as received, between 1050 and 1300 °C, to simulate the soft-, medium- and dead-burning conditions occurring in Twin-Shaft Regenerative (TSR) kilns. The raw materials and burnt products were characterized based on a multidisciplinary analytical approach, including physical-chemical, mineralogical-petrographic, crystallographic and thermal analyses. The lime reactivity was determined according to the European slaking test method. By means of statistical analysis of different datasets, key factors controlling the lime reactivity and overburning tendency at high temperature could be identified.

TEXT G. Vola [1-2], L. Sarandrea [1], M. Mazzieri [2], P. Bresciani [1], M. Ardit [2], G. Cruciani [2]

[1]Cimprogetti Srl Lime Technologies, Dalmine/Italy
[2]Physics and Earth Sciences Department, University of Ferrara, Ferrara/Italy

All authors

Reactivity and overburning tendency of quicklime burnt at high temperature

1 Introduction

The reactivity of commercial lime became a matter of considerable interest with the introduction of the basic oxygen converter steel furnace during the 1950s [1]. The use of quicklime instead of limestone and the rapid acceptance of this technology during the 1960s caused the definitive substitution of open-hearth steelmaking furnaces, and created parallel a revolution within the lime industry [2]. Nowadays, lime reactivity plays a critical role in different industrial processes. It is especially important to make a good slag facilitating the removal of sulphur and phosphorus and for providing a safer platform to withstand high-intensity arc plasma in the electric arc furnace, and violent reactions in the basic oxygen furnace [3]. Lime reactivity is also required as a fundamental process parameter in several industrial sectors including the constructions, chemical, mining, agricultural, geotechnical, pharmaceutical, environmental and alimentary sectors, i.e. for removing impurities, as a fluxing or leaching agent, as well as, for acid neutralization, pH sta-

bilization and flue gas desulphurization [4]. Lime reactivity in the building lime sector is traditionally evaluated according to water slaking rate tests [5-6]. Pioneering studies on lime reactivity were performed during the 1970s under the auspices of the US National Lime Associations [7-8]. Since the beginning of the 2000s, several studies have pointed out the effect of particle size distribution, calcination kinetics, specific surface area, apparent density and impurity content [9-11]. Over the last ten years, an increasing number of mineralogical, petrographic and crystallographic studies have been performed, to bridge the geological gap. Geoscientists have proposed studies based on microfacies analysis, petrophysical properties and crystallographic characterization of carbonate rocks and derived burnt products [12-19].

Nowadays, Twin Shaft Regenerative (TSR) kilns, are generally considered the best technology to achieve the goal of soft-burnt reactive quicklime with different types of fuels [20]. In particular, TSR kilns present the lowest specific energy consumption compared with other types
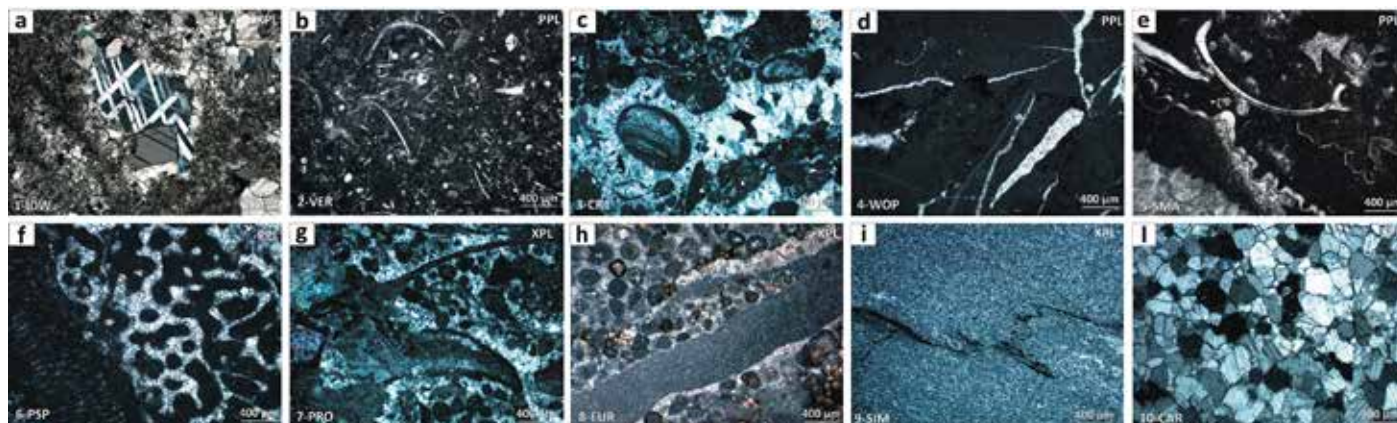
1 Petrographic analysis of carbonate rocks
Symbols legend: Plane Polarized Light (PPL); Crossed Polarized Light (XPL)

1a Microbial boundstone with clotted peloidal micrite-microsparite associated with large mm-sized equant and poikilotopic twinned calcite cement (1-IDW)

1b Nodular ammonite-bearing pelagic wackestone with thin-shelled bivalves, ostracods, pelagic foraminifera, i.e. protoglobigerins, and radiolarians (2-VER)

1c Subtidal-intertidal peloidal-fossiliferous packstone/grainstone passing to pisolitic rudstone, presenting fibrous-radial and equant calcite cements filling the intraclastic porosity (3-CR1)

1d Subtidal mudstone/wackestone with rare ostracods. Tensional fractures filled in by clear mosaic calcite cements (4-WOP)

1e Kerogen-rich floatstone/rudstone from different stromatoporoidal lithofacies. The fossiliferous content includes conodont, trilobites, large bivalves and rugose corals floating into abundant micritic matrix (5-SMA)

1f Reefoidal framestone/rudstone characterized by bryozoan-foraminifera-Corallinacean red algae association. Intraclastic porosity filled in by equant calcite cements (6-PSP)

1g Peloidal-fossiliferous packstone/grainstone with rugose corals, large bivalves and gastropods. Diagenetic dolomite replacements (7-PRO)

1h Coated-grain peloidal grainstone/packstone associated with mm-sized micritic intraclasts of rectangular shape, i.e. flat pebble conglomerate (8-EUR)

1i Very fine-grained calcitic marble with well-developed schistosity, grain orientation and sporadic stylolites (9-SIM)

1j Medium-up to coarse-grained calcitic marble with straight grain boundaries and no visible orientation (10-CAR)

of kilns owing to the regenerative process [21]. Indeed, TSR kilns represent the best compromise for lowering costs, reducing gas emissions, and limiting environmental impact. According to Cimprogetti's expertise, the production of soft-burnt quicklime in TSR kilns firing solid fuels, i.e. coal and petcoke, is a critical task.

Therefore, the main goal of this study was to investigate the burnability of different calcium carbonate rocks supplied in the typical crushed fractions, considering the range of temperature occurring in TSR kilns firing solid fuels. Rock samples with different geological origin, stratigraphic position, fabric and composition were supplied from producers worldwide. Multidisciplinary research was carried out to investigate heating behaviour, overburning tendency and quicklime reactivity. Moreover, the calcination kinetics were determined by means of thermal analysis on massive samples. Finally, the BET surface area and crystallographic parameters of the lime were considered, too. The statistical analysis allowed the evaluation of correlations between different data-sets and the slaking reactivity. Results put further constraints on the suitability of different carbonate rocks for lime manufacture in TSR kilns using solid fuels.

2 Tests and methods
2.1 Mineralogical-petrographic and crystallographic analyses
The microfacies analysis of carbonate rocks according to their depositional textures and diagenetic modifications was performed in compliance with [22]. Crystal fabric analyses allow marble types and deformation styles to be distinguished, too. The identification of mineralogical phases was performed by means of X-ray powder diffraction analysis (XRD). Moreover, the quantitative phase analysis was carried out using the Rietveld method [23].

2.2 Burning trials, thermal analysis and slaking tests
Burning trials were carried out on rock samples as received in an electric muffle furnace under

air conditions. Burning temperatures between 1050 – 1300 °C were considered for simulation of the calcination process in TSR kilns using different kinds of fuels. The thermal analysis was performed on massive rocks in a thermogravimetric muffle furnace at 1200 °C. Calcination parameters were extrapolated according to the Fuoss–Salymer–Wilson method, as reported by [18]. The lime reactivity was evaluated with the European slaking test [6]. According to the practice commonly used by lime producers, "high reactivity" is when ΔT 40 °C or t_{60} < 3 min, "medium reactivity" when t_{60} is between 3 to 6 min, and "low reactivity" when t_{60} > 6 min.

2.3 BET specific surface area and real density

The porosity of burnt limes was investigated by means of nitrogen absorption using a gas sorptometer. Especially, the specific surface area and the volume of monolayer coverage were determined according to the BET theory. The analysis of real density was performed with helium pycnometry.

3 Results
3.1 Characterization of carbonate rocks and burnt limes

Preliminary geological information, origin, formation, lithology and fabrics are reported in Table 1. Selected samples, mostly high-calcium

Sample Name	Stratigraphic position	Geological unit or formation	Provenance	Lithology i.e. macroscopic description	Rock fabric i.e. petrographic analysis	Fraction	References
1-IDW	Precambrian, Neoarchean (2520 Ma)	Uppermost Kogelbeen Fm. or Lower Gamohaan Fm.	Ouplass Mine, Daniëlskuil, South Africa	Light and dark grey to black microbial limestone enriched in organic carbon	Microbial boundstone with laminated clotted peloidal micrite recrystallized into microsparite, associated with herringbone marine calcite. Diagenetic features include stylolites, organic carbon (kerogen), saddle dolomite and very large cm-sized poikilotopic calcite cements.	40-80 mm 30-50 mm	[17]
2-VER	Middle Jurassic (176-161 Ma)	Rosso Ammonitico Veronese Fm.	Valpolicella quarry district, Verona, Italy	Reddish nodular ammonite-bearing pelagic micritic limestone, i.e. mud-supported lithofacies	Wackestone/packstone with planktonic thin-shelled bivalves, ostracods, foraminifera (protoglobigerins) and radiolarians. Stylolites and solution seams due to pressure solution. The impurity content is about 2 %	15-30 mm	[18]
3-CR1	Latest Ladinian-Early Carnian (228 Ma)	Lower portion (depocentral) of the Calcare Rosso limestone Fm.	Cadei quarry, middle Brembana Valley, Camerata Cornello, Bergamo, Italy	Medium to dark grey and black peritidal, mainly sub-intertidal, limestone locally passing to neomorphic cement, including dm-sized fibrous-radial early diagenetic calcite, i.e. "raggioni", deformed antiformal structures, i.e. cm-sized (embryo) up to m-sized (senile) tepees and grey-coloured diagenetic-pedogenetic breccias	Fossiliferous sub-intertidal burrowed wackestone-packstone associated with supratidal pisolitic grainstone-rudstones. Diagenetic features include: early diagenetic fibrous-radial calcite, senile up to mature tepees, terra-rossa paleosoils and pedogenetic breccias.	40-80 mm	[27]
4-WOP	Upper Triassic (217-200 Ma)	Dachsteinkalk Fm.	Dürnbach quarry, Waldegg, Austria	Light to medium dark grey peritidal limestone, mainly constituted of sub-intertidal facies locally passing to supratidal facies enriched in "terra-rossa" paleosoils and polychromous marly limestones. Diagenetic antiformal structures, i.e. tepees	Mudstone/wackestone with rare fossiliferous content (ostracods), locally passing to poorly washed packstone-grainstone. Secondary tensional fractures filled in by clear and twinned mosaic cement. Stylolites and solution seams postdate fractures.	30-50 mm 40-70 mm	[19]
5-SMA	Silurian, Lower Wenlock (428-423 Ma)	Hangvar Fm.	Storugns quarry, Gotland island, Sweden	Yellowish brown to olive grey massive carbonates, mostly of reefoidal origin, with organic matter and interbedded siliciclastic sediments. Fossiliferous grain-supported facies locally passing to lacustrine mud-supported ones.	Fossiliferous kerogen-rich floatstone/rudstone locally passing to packstone/wackestone from different stromatoporoidal facies including reef front, reef core, inter-reef, shoal and back-reef environments. Large mm-sized faunas including conodonts, rugose corals, possible trilobites, brachiopods and bivalves. Intraclastic porosity filled in by equant and poikilotopic calcite cement. The impurity content is about 5 %	50-70 mm 30-50 mm	[18]

carbonates, cover a large part of the geological time–scale, ranging from the Neoarchean (2520 Ma) era up to the Eocene (34 Ma) epoch. The most significant rock fabrics are shown in Figure 1. The mineralogical analysis shows that some samples are slightly dolomitic in composition; some others are enriched in quartz and/or clay minerals (Table 2). Burnt limes from slightly dolomitic limestones typically present a significant content of periclase (MgO) associated with lime (CaO). Cementitious mineral phases, such as di–calcium silicate or larnite (Ca_2SiO_4), tri–calcium silicate or hatrurite (Ca_3SiO_5), aluminate phase ($Na_{2x}Ca_{3-x}Al_2O_6$), and ferrite or brownmillerite ($Ca_2(Al_x,Fe_{1-x})_2O_5$) are present as associated constituents in moderately hydraulic limes from slightly impure carbonates. Moreover, limes from South African microbialites presented a significant content of di–calcium manganate $Ca_2(MnO_4)$ [17]. Detailed chemical–physical, mineralogical–petrographic analyses of burnt limes are available in [19].

## 3.2 Thermal behaviour characterization and slaking reactivity

Results from thermogravimetric analysis showed significant differences in calcination rates. The highest (apparent) activation energy, calcination velocity and starting calcination time/tempera-

Sample Name	Stratigraphic position	Geological unit or formation	Provenance	Lithology i.e. macroscopic description	Rock fabric i.e. petrographic analysis	Fraction	References
6-PSP	Eocene (?)	Nd	Karawang quarry, Rembang, Java, Indonesia	White porous massive limestone presenting encrusting lithofacies	Framestone/rudstone characterized by encrusting bryozoan-foraminifera-red algae association. Primary intraclastic porosity partially filled in by mosaic calcite cement.	40-80 mm 30-60 mm	[19]
7-PRO	Palaeozoic (?)	Nd	St Petersburg, Russia	Yellowish grey fossiliferous limestone presenting mud-supported and grain-supported lithofacies	Peloidal-fossiliferous packstone/grainstone and mm-sized mosaic calcite cements associated with subordinated poorly washed packstone. Abundant benthic fauna (40-50%), i.e. rugose corals, bivalves, gastropods. Diagenetic microsparite and saddle dolomite replacements.	40-80 mm	[19]
8-EUR	Cambrian-Ordovician (c.488 Ma)	Shoshka-bulakskaya stratigraphic succession	Ulken-Aktau deposit, Zhanatas, Zhambyl, Kazakhstan	Multicoloured flat-pebbles breccia laterally passing to light to medium grey micritic and dolo-micritic limestone	Flat-pebbles rudstone associated with coated grains peloidal grainstone/packstone and subordinated wackestone. Diagenetic features include double-steps dolomite associated with blocky and poikilotopic cements and sporadic chalcedony replacements	20-40 mm (cores)	[19]
9-SIM	Nd	Nd	Târgu Jiu, Gorj, Romania	Fine and very fine-grained granoblastic marble, characterized by a well-developed schistosity and homogeneous grey colour	Primary texture completely obliterated by pervasive metamorphic recrystallization. Very fine-grained oriented granoblastic microstructure, with sporadic larger twinned subhedral crystals. Appreciable grain orientation.	40-80 mm	Nd
10-CAR	Lower Jurassic (196-176 Ma)	Apuane Metamorphic Complex, Marble s.s. Fm.	Carrara quarry district, Massa-Carrara, Italy	Fine to medium coarse-grained metalimestone, i.e. granoblastic marble, homogeneously pearl-white coloured or with grey tiny spots	Granoblastic microstructures depending on two main tectonic deformation phases. Well-defined, straight or slightly curved grain boundaries with no optical evidence of crystal plastic deformation. Subordinated xenoblastic structures with less defined grain boundaries, sometimes sutured or embayed to lobate. Variable grain-size and sometimes appreciable grain orientation.	15-30 mm	[18]

2 Slaking reactivity according to UNI EN 459-2 (sample IDW)
2a Slaking rates at different burning temperatures
2b Differential slaking rates at different burning temperatures
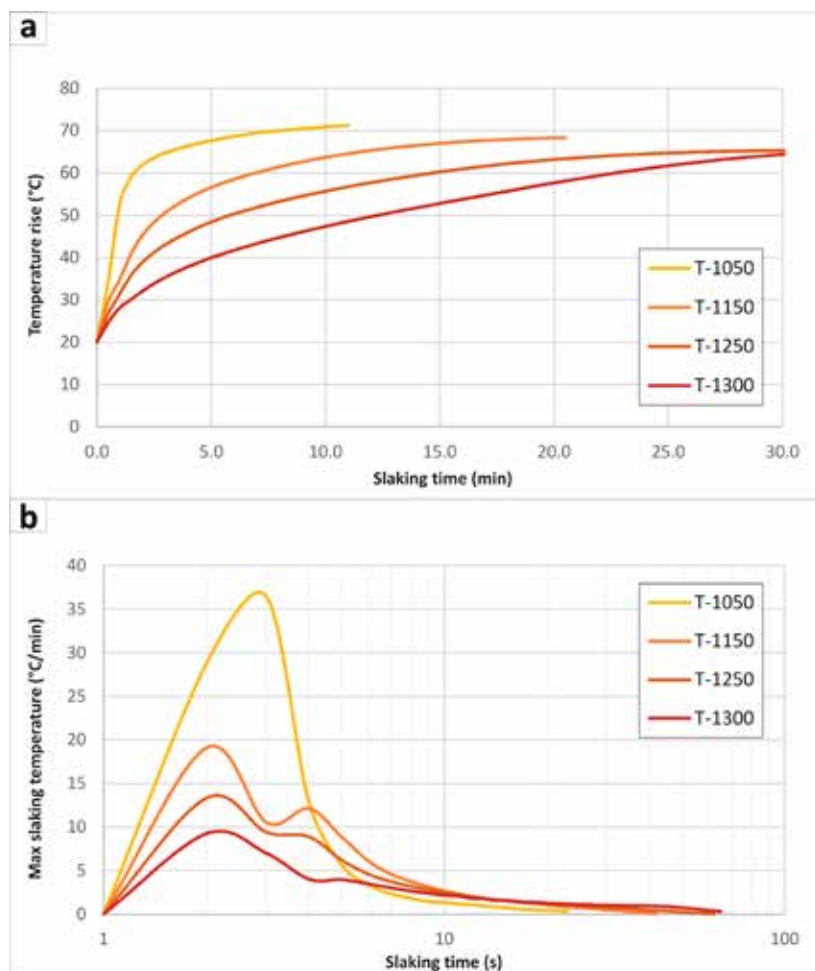
ture were observed for the coarse-sized grano-blastic marble from Carrara (CAR). Conversely, the lowest (apparent) activation energy, calcination velocity and starting calcination time/temperature were observed for the micritic marly limestone from Verona (VER), respectively (Table 3). Results of the slaking tests, in terms of temperature rise, t_{60}, and the maximum slaking temperature, T_{max}, are reported in Table 4. An example of slaking rates of limes burnt at different T is reported in Figure 2. Soft-burnt limes at 1050 °C showed a t_{60} from 0.4 – 2.2 min; medium-burnt limes at 1150 °C showed a t_{60} from 0.5 – 10.9 min and, finally, dead-burnt limes at 1250 °C showed a t_{60} from 1.3 – 22.2 min. At the same time, the T_{max} ranged between 82.7 and 70.5 °C for soft-burnt limes at 1050 °C, between 79.2 and 66.0 °C for medium-burnt limes at 1150 °C, and between 79.2 to 63.6 °C for dead-burnt limes at 1250 °C. The coralline limestone from Indonesia (PSP) presented the highest reactivity at 1050 °C (t_{60} = 0.3 min, T_{max} = 85.5 °C), while the stromatoporoidal limestone from Sweden (SMA) presented the lowest reactivity at the same temperature (t_{60} = 2.2 min, T_{max} = 70.6 °C). On the other hand, the fine-grained marble from Romania (SIM) presented the highest reactivity at 1250 °C (t_{60} = 1.3 min, T_{max} = 79.2 °C), while the microbialite from South Africa (IDW) the lowest reactivity at the same temperature (t_{60} = 22.2 min, T_{max} = 63.5 °C).

4 Discussion
### 4.1 Impact of rock fabric and impurity content
The burning temperature is one of the most important process parameters affecting lime slaking [4].

Table 2a Quantitative phase analysis (XRD-QPA) of selected carbonate rock samples. Symbols legend of fundamental mineralogical phases: Cal: calcite, $CaCO_3$; Dol: dolomite, $CaMg(CO_3)_2$. Associated mineralogical phases: Ank: ankerite, $Ca(Fe^{2+},Mg,Mn)(CO_3)_2$; Qtz: quartz, SiO_2; Ms/Ill: muscovite, $KAl_2(Si_3Al)O_{10}(OH,F)_2$, or illite, $(K,H_3O)(Al,Mg,Fe)_2(Si,Al)_4O_{10}[(OH)_2,(H_2O)]$; Clc: clinochlore, $(Mg,Fe^{2+})_5Al(Si_3Al)O_{10}(OH)_8$; Mnt: montmorillonite, $(Na,Ca)_{0.3}(Al,Mg)_2Si_4O_{10}(OH)_2·n(H_2O)$; Gt: goethite, $Fe^{3+}O(OH)$. Tr: traces (<0.5 %)

Name	Cal (wt.%)	Dol (wt.%)	Ank (wt.%)	Qtz (wt.%)	Ms/Ill (wt.%)	Mnt (wt.%)	Clc (wt.%)	Kfs (wt.%)	Gt (wt.%)
1-IDW	98.3	1.5	-	Tr	Tr	-	Tr	-	-
2-VER	98.0	-	-	Tr	1.1	-	-	Tr	Tr
3-CR1	89.5	8.5	-	1.0	1.0	-	-	-	-
4-WOP	98.3	2.8	-	Tr	Tr	-	-	-	-
5-SMA	95.1	-	-	1.4	1.4	Tr	1.9	-	-
6-PSP	99.9	-	-	Tr	-	-	-	-	-
7-PRO	98.0	1.8	-	-	-	-	-	Tr	-
8-EUR	84.8	14.3	1.0	0.9	-	-	-	-	-
9-SIM	99.9	-	-	-	Tr	-	-	-	-
10-CAR	99.1	0.8	-	-	Tr	-	-	-	-

Table 2b Available Lime Index (ALI) and Quantitative Phase Analysis (XRD-QPA) of lime samples burnt at different T. Symbols legend of fundamental phases: Lime, CaO; Per: periclase, MgO. Associated phases: Lar: larnite, Ca_2SiO_4; Hat: hatrurite, Ca_3SiO_5; Aln: aluminate phase, $Na_{2x}Ca_{3-x}Al_2O_6$; Brw: brownmillerite, $Ca_2(Al_x,Fe_{1-x})_2O_5$; Ca_2MnO_4: di-calcium manganate; Cal: calcite; Qtz: quartz. Alteration phase: Por, portlandite $Ca(OH)_2$. Tr: traces (<0.5 %). QPA values are the average of two different determinations

Sample	T	ALI	Lime	Per	Lar	Hat	Aln	Brw	Ca_2MnO_4	Cal	Qtz	Por
	(°C)	(Wt.%)	(Wt.%)	(Wt.%)	(Wt.%)	(Wt.%)	(Wt.%)	(Wt.%)	(Wt.%)	(Wt.%)	(Wt.%)	(Wt.%)
1-IDW	1050	95.2	91.9	1.5	Tr	Tr			5.8	0.8		Tr
	1150	95.6	95.3	0.7	Tr	Tr			4.1			Tr
	1200	90.7	95.3	1.6	0.6	Tr	Tr		2.2	Tr		Tr
	1250	93.6	94.2	1.2	Tr	1.6	Tr		3.2			Tr
2-VER	1050	89.7	90.6	Tr	6.6	1.4	1.2					Tr
	1150	90.1	89.0	Tr	10.0		Tr	2.1				Tr
	1250	89.0	91.9	1.0	7.1							Tr
3-CR1	1050	85.1	85.5	3.0	5.0	2.6	0.5	2.7		Tr	0.7	Tr
	1150	83.5	88.4	2.6	5.2	0.9	0.8	2.2				Tr
	1250	81.8	79.5	3.1	8.3	6.7	1.3	0.9		Tr		Tr
4-WOP	1050	91.8	95.4	1.8	Tr	2.0	1.0			Tr		Tr
	1150	90.8	95.4	2.1	1.0	1.0	0.7			Tr		Tr
	1200	95.8	96.9	1.0	1.7		0.5					Tr
	1250	94.4	96.5	0.9	1.6	Tr	0.7					Tr
	1300	96.1	95.9	1.4	1.9	0.7	Tr					Tr
5-SMA	1050	90.6	95.5	0.7	2.9	Tr	0.5					Tr
	1150	87.8	94.4	1.1	1.9	Tr	1.9					Tr
	1200	93.9	96.7	0.5	1.8	Tr	1.0			Tr		Tr
	1250	92.2	96.4	0.6	2.7	Tr	0.6					Tr
	1300	96.3	97.2	0.8	1.5	0.6	Tr					Tr
6-PSP	1050	98.1	100	Tr								Tr
	1150	98.0	100	Tr	Tr		Tr					Tr
	1200	98.1	99.6	Tr			Tr			Tr		Tr
	1250	98.0	99.0	Tr	Tr	Tr	Tr			Tr		Tr
7-PRO	1050	96.7	95.0	0.5	1.2	0.8	2.5					Tr
	1150	91.1	96.0	1.8			1.7					Tr
	1250	97.3	96.9				1.8					Tr
8-EUR	1050	90.9	96.8	1.7	0.7	0.4	Tr				Tr	Tr
	1150	89.5	95.0	0.7	0.6	2.8	1.0					Tr
	1200	83.4	92.8	3.2	2.3	0.5	1.4					Tr
	1250	83.0	89.4	3.1	2.2	1.6	1.6					Tr
9-SIM	1050	94.5	99.5	0.5								Tr
	1150	93.1	98.9	0.5				Tr				Tr
	1300	87.3	97.0	1.0	1.0	1.0						Tr
10-CAR	1050	90.1	98.6	1.4			Tr					Tr
	1150	93.9	98.8	1.2			Tr					Tr
	1250	94.0	98.0	1.1			1.0					Tr
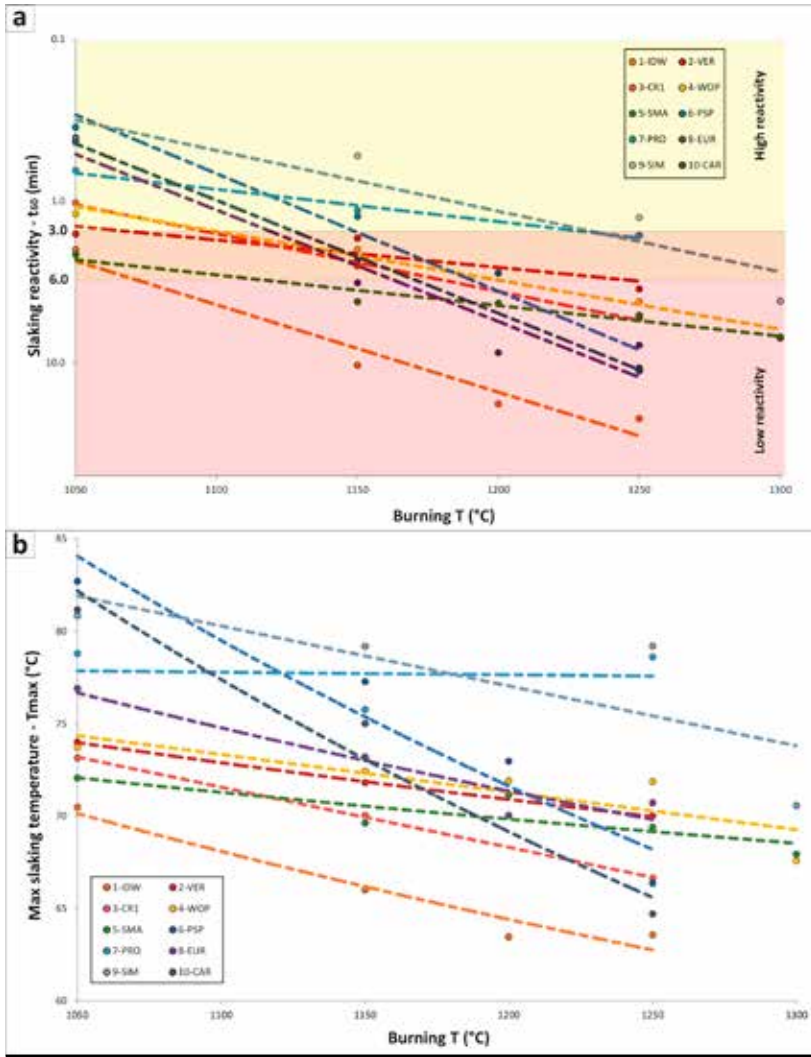
3 Slaking reactivity plots vs burning temperature

3a Temperature rise, i.e. $\Delta T40°C$ or t_{60} (min) versus burning temperature (°C)
3b Maximum slaking temperature, T_{max} (°C) versus burning temperature (°C)
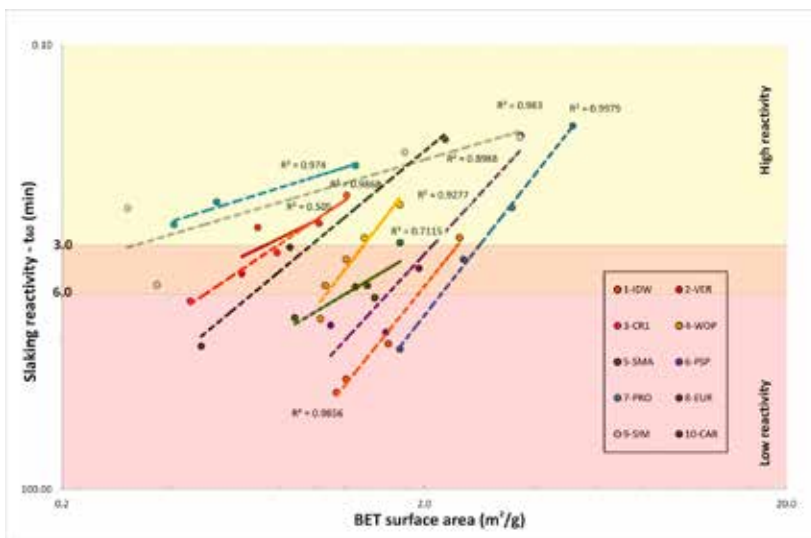
4 Plot of slaking reactivity, i.e. temperature rise (ΔT 40 °C or t_{60}) versus BET surface area (m²/g). Correlation factors of each sample are reported

Effectively, the statistical analysis indicated the inverse correlation between the slaking reactivity and the burning temperature (Figure 3). Moreover, the deeper the slope of the slaking curves is, the higher is the overburning tendency at high temperature. Significant differences in slaking rates and overburning tendency can be firstly related to different rock fabrics and impurity content, i.e. different mineralogical-petrographic compositions. Based on this evidence, samples can be divided into four main groups, as follows:

1) The first group is represented by samples presenting very high reactivity at 1050 °C and very low reactivity at 1250 to 1300 °C. These samples showed the highest overburning tendency, testified by the deepest slope of the slaking curves in Figure 3. The samples are characterized by large calcitic fabrics, i.e. coralline limestone with mosaic calcite cement fillings (PSP) and coarse-grained marble (CAR), associated with very low impurity content

2) The second group is represented by samples presenting very high reactivity at 1050 °C and high- medium-high reactivity at 1250 to 1300 °C. These samples showed a low overburning tendency, testified by the gentle slope of the slaking curves in Figure 3. The samples are characterized by fine-grained calcite fabrics, i.e. fossiliferous packstone/grainstone associated with diagenetic microsparite (PRO) and fine-grained calcitic marble (SIM) with low impurity content

3) The third group is represented by one sample presenting medium-high reactivity at 1050 °C and very low reactivity at 1150 to 1300 °C. This sample showed a very high overburning tendency, testified by the deep slope of the slaking curves in Figure 3. This is the South African microbial boundstone (IDW) associated with medium-high impurity content

4) The fourth group is represented by samples presenting medium-high reactivity at 1050 °C and medium-low reactivity at 1250 to 1300 °C. These samples showed the lowest overburning tendency, testified by the gentle slope of the slaking curves in Figure 3. These samples are characterized by fine-grained fabrics, i.e. mainly mud-supported or micritic limestones (VER, CR1, WOP, SMA) associated with medium-high impurity content, i.e. quartz and clays scattered within the micritic matrix and sporadic diagenetic dolomite replacements

A summary of this classification is reported in Table 5. Limits between different groups are not strictly defined because of the large variability of geological or intrinsic rock parameters. Some important remarks can be derived, as well:

1) Medium- up to coarse-grained marbles, grain-supported and coralline limestones, characterized by large calcite cement fillings or replacements, are affected by the overburning tendency more than fine-grained marbles and/or mud-supported or micritic limestones. Lime particles produced by decomposition of coarser-grained rock fabrics appear more prone than finer-grained ones to coarsening and sintering. This fact is consistent with data from the thermal analysis, i.e. the kinetics parameters extrapolated from thermogravimetric analyses on massive samples. Moreover, it is in line with the pseudomorphic and topotactic calcination reactions reported by [13] and other studies on the effect of "limestone microstructure", i.e. rock fabric, on the (apparent) activation energy [15, 17–18]

2) The impurity content is a key factor at T > 1250 °C, controlling the formation of different cementitious minerals, i.e. larnite, hatrurite, brownmillerite and aluminate phase [24]. Cementitious minerals slake at higher rates in respect of the sintered dead-burnt lime. Moreover, they form a boundary layer between lime crystallites, acting as sintering inhibitors at high temperature [10]. This is the reason why hydraulic limes showed lower overburning tendency than pure limes at high temperature.

4.2 Impact of quicklime physical parameters
Derived physical-chemical, mineralogical and microstructural parameters also affect the quicklime reactivity [4]. Effectively, experimental data confirmed the significant impact of the BET surface area and the real density on slaking rates. The correlation between the slaking reactivity, i.e. t_{60}, and the BET surface area is reported in **Figure 4**. Trends are consistent with expectations, but absolute values for the BET area are sometimes not comparable between samples of different origin. The Russian sample PRO, for instance, showed very high reactivity at 1150 to 1250 °C, which is apparently not congruent with very low values for the BET area. Conversely, other samples presenting lower slaking rates at the same temperature, exhibit higher values for BET area. Unexpected and substantially unexplained results have already been reported in the literature [25]. Moreover, the statistical analysis indicated the inverse correlation between the BET area and the real density based on gas pycnometry (**Figure 5**). This is consistent with the expectations and results reported in [18].

## 4.3 Analysis of lime crystallographic and microstructural parameters
The lime (CaO) lattice parameter (crystal system, cubic) was plotted against the burning temperature and the slaking reactivity. A well-defined inverse

correlation is observed between the Rietveld refined lime lattice parameter a (Å) and the burning temperature (°C) (**Figure 6**). General trends of lattice contraction at high temperature occur for all samples. This evidence has already been reported in the literature [26], but no clear explanation has been provided. We suggest that the observed contraction of the lime unit-cell can be interpreted taking into account the temperature-dependent miscibility gap between CaO and MgO. In fact, the incorporation of smaller Mg^{2+} ions (ionic radius 0.72 Å) replacing larger Ca^{2+} ions (ionic radius 1.00 Å) in the lime lattice is increased with increas-

Table 3 Crystallographic data of the lime by Rietveld refinement method and other physical parameters of burnt lime samples. Symbols legend, a: lime lattice parameter; Er: error; BET: specific surface area by BET method, Density: real density by helium pycnometry

Sample	T	a	Er	BET	Density
	(°C)	(Å)	(Å)	(m²/g)	(g/cm³)
1-IDW	1050	4.80978	11	2.50	3.25
	1150	4.80857	2	1.59	3.30
	1200	4.80853	2	1.22	3.32
	1250	4.80793	3	1.14	3.32
2-VER	1050	4.81059	3	1.02	3.19
	1150	4.80881	4	0.69	3.22
	1250	4.80767	3	0.63	3.22
3-CR1	1050	4.81051	3	1.22	3.28
	1150	4.80869	4	0.78	3.29
	1250	4.80702	4	0.45	3.32
4-WOP	1050	4.81015	3	1.71	3.23
	1150	4.80855	2	1.37	3.28
	1200	4.80782	3	1.22	3.28
	1250	4.80692	3	1.07	3.29
	1300	4.80776	4	1.03	3.30
5-SMA	1050	4.80998	3	1.71	3.11
	1150	4.80927	3	1.39	3.14
	1200	4.80797	4	1.29	3.19
	1250	4.80733	3	1.46	3.22
	1300	4.80793	3	0.88	3.29
6-PSP	1050	4.81256	4	5.15	3.03
	1150	4.81258	4	3.49	3.10
	1200	4.81042	3	2.57	3.18
	1250	4.81013	2	1.71	3.29
7-PRO	1050	4.81053	3	1.29	3.29
	1150	4.80991	5	0.53	3.35
	1250	4.80939	5	0.41	3.35
8-EUR	1050	4.81017	3	3.69	3.09
	1150	4.80910	4	1.93	3.18
	1200	4.80895	3	1.57	3.25
	1250	4.80774	5	1.10	3.29
9-SIM	1050	4.81010	4	3.68	3.26
	1150	4.80844	4	1.77	3.30
	1250	4.80719	4	0.30	3.32
	1300	4.80637	4	0.37	3.34
10-CAR	1050	4.80951	2	2.29	3.19
	1150	4.80850	2	0.85	3.24
	1250	4.80683	3	0.48	3.27
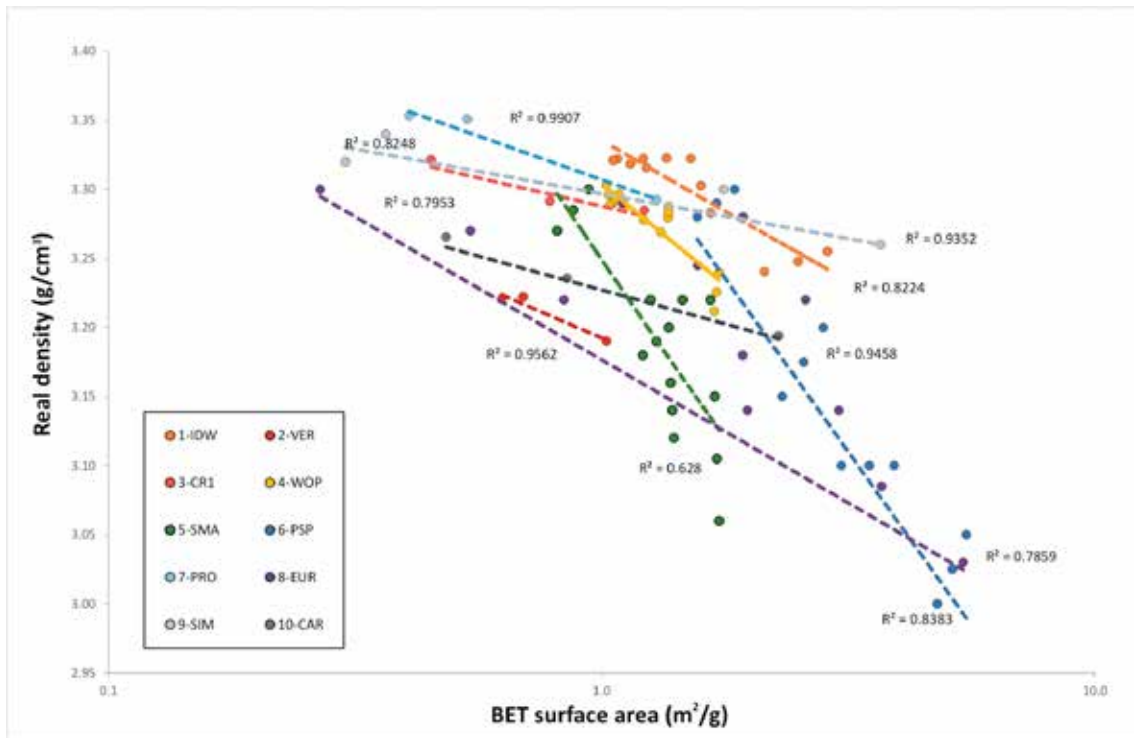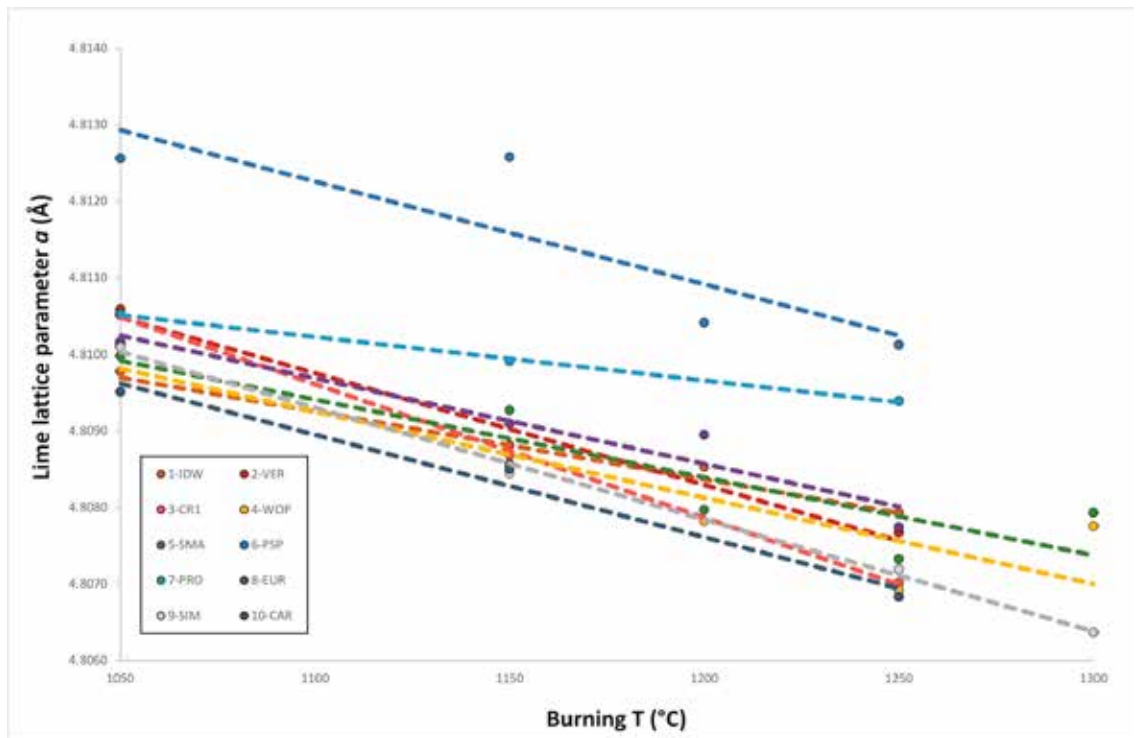
ing firing temperature, thus explaining the contraction. From the technological point of view, a larger amount of Mg incorporated in CaO would contribute to a decrease of reactivity owing to the low hydration kinetics of the periclase to form brucite, $Mg(OH)_2$, at room pressure [4].

5 Conclusion

This study allowed the investigation of the burnability, overburning tendency, and lime slaking reactivity of carbonate rocks in the typical range of temperatures occurring in a TSR kiln firing solid fuels (1150 to 1300 °C). Crushed rock fractions were submitted to burning and slaking tests. A multidisciplinary analytical approach, including chemical-physical, mineralogical-petrographic, crystallographic and thermal analyses, was carried out on raw materials and burnt products.

The first part of the study allowed identification of the rock fabric and the impurity content, i.e. the mineralogical-petrographic composition, as key factors controlling the slaking rates and

Sample	UM	1-IDW	2-VER	10-CAR
Sample mass	g	131.3	132.0	131.8
LOI	%	44.1	43.4	44.1
Starting time	min	61.5	59.0	57.8
Max time	min	96.3	98.5	98.8
Ending time	min	130.8	128.0	135.8
Δt	min	69.4	69.0	78.0
Starting temperature	°C	697.9	688.0	717.0
Max temperature	°C	1026.1	1083.0	1125.0
Ending temperature	°C	1198.5	1200.0	1200.0
ΔT	°C	500.6	512.0	483.0
Activation energy (Ea)	KJ/mol	79.3	77.4	99.1
Time factor (A)	1/s	3.1E+05	9.2E-01	4.2E+00
Constant reaction (K)	1/s	8.7E-04	8.7E-04	9.0E-04

Table 4 Kinetics parameters from TG-DTG analysis according to FSW method on massive (ca. 130 g) samples burnt at 1200 °C (preliminary results). The sample 1-IDW represents the average of 7 representative samples from the same quarry (see [17])

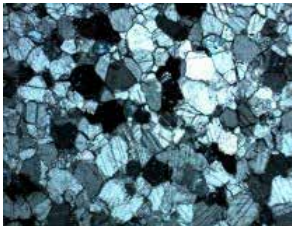| Sample	T	ΔT 40 °C or t_{60}		T_{max}	t_{max}	HR_{max}
	(°C)	(min)	(sec)	(°C)	(min)	(°C/min)
1-IDW	1050	2.0	120.0	70.5	9.5	31.2
	1150	10.4	624.0	66.0	22.3	17.6
	1200	18.0	1080.0	63.5	30.0	13.8
	1250	22.2	1332.0	63.6	31.5	11.1
2-VER	1050	1.6	96.0	74.0	5.2	70.0
	1150	1.7	102.0	71.8	4.5	27.4
	1250	3.5	210.0	70.0	8.5	23.8
3-CR1	1050	1.0	61.8	73.1	5.6	161.5
	1150	2.5	151.5	70.0	15.3	30.8
	1250	5.3	320.8	66.6	20.5	20.4
4-WOP	1050	1.2	72.0	73.7	4.5	41.0
	1150	2.0	120.0	72.4	11.0	26.0
	1200	2.8	168.0	71.9	14.8	20.0
	1250	4.2	252.0	71.9	15.5	17.0
	1300	7.1	423.0	67.6	21.0	17.0
5-SMA	1050	2.2	129.0	72.1	6.8	25.1
	1150	4.2	252.0	69.6	10.5	19.5
	1200	4.3	258.0	71.1	11.5	17.5
	1250	5.1	306.0	69.4	11.0	16.5
	1300	7.0	417.0	67.9	18.0	14.1
6-PSP	1050	0.4	21.0	82.7	3.0	111.0
	1150	1.3	75.0	77.3	9.5	68.0
	1200	2.8	168.0	73.0	11.8	33.0
	1250	11.3	678.0	66.4	25.0	18.0
7-PRO	1050	0.6	39.0	78.8	5.0	70.9
	1150	1.1	69.0	75.8	12.5	45.3
	1250	1.6	98.0	78.6	8.5	27.9
8-EUR	1050	0.4	24.4	76.9	4.0	98.1
	1150	3.2	192.8	73.2	48.3	50.3
	1200	8.7	521.2	70.0	25.5	32.1
	1250	7.8	468.3	70.7	30.6	Nd
9-SIM	1050	0.4	25.0	80.8	6.5	100.8
	1150	0.5	32.0	79.2	8.0	78.5
	1250	1.3	76.0	79.2	12.5	35.5
	1300	4.2	250.0	70.6	21.5	23.6
10-CAR	1050	0.4	26.0	81.2	12.5	92.4
	1150	2.3	139.0	75.0	27.5	47.6
	1250	10.8	648.0	64.7	34.5	27.8

Table 5 Slaking reactivity of limes burnt at 1050 – 1300 °C

the overburning tendency of the lime at high temperature. Especially, coarse-sized granoblastic marbles, grain-supported and coralline limestones, presenting calcite cement fillings and/or replacements, are affected by higher overburning tendency than fine-grained marbles and/or mud-supported or micritic limestones. Moreover, hydraulic limes showed higher reactivity than pure limes at high temperature. This fact has to be related to the formation of different cementitious minerals at T > 1250 °C, which slake at higher rates than the dead-burnt lime. Moreover, they could act as sintering inhibitors for the lime at high temperature [10]. Results from calcination kinetics analysis performed on massive samples allowed the conclusion that the higher the grain/crystal sizes of carbonate rocks are, the higher are the (apparent) activation energy, the calcination velocity, the starting calcination time/temperature and the slaking reactivity. This is consistent with a previous study performed on massive granulated samples reported by [18], and pseudomorphic and topotactic calcination reactions reported by [13].

The second part of the study allowed identification of the impact of lime physical-chemical and mineralogical-crystallographic parameters on slaking reactivity. The statistical analysis indicated the direct correlation between BET surface area and the temperature rise, i.e. t_{60}, which is also consistent with the lime densification at high temperature. The contraction of the lime unit-cell as a function of temperature and bulk Mg content is readily explained by the higher incorporation of Mg in the CaO lattice. The higher miscibility of MgO with CaO crystal structure at 1300 °C is also consistent with a lower slaking reactivity of the lime product, considering that the hydration kinetics of periclase at room pressure is extremely low.

Table 6 Combination of main different variables, i.e. rock fabric, impurity content and slaking reactivity, allows identification of four main groups of rocks with different overburning tendency (OT) at high temperature (HT). The indicative impurity content is from the quantitative phase analysis (XRD-QPA)

Group	Rock fabric	Representative micrographs	Impurity content	Reactivity at 1050 °C	Reactivity at 1250 °C	OT at HT	Samples
1	Coarse-sized granoblastic marbles, grain-supported and other massive limestones		very low (0.5%)	very high (explosive) i.e. t_{60} < 1 min	very low i.e. t_{60} > 10 min	very high OT (deep slope Plot 3)	PSP, CAR
2	Fine-grained marbles and grain-supported limestones		very low (< 0.5 %)	very high (explosive) i.e. t_{60} < 1 min	medium-high i.e. t_{60} 2-4 min	low OT (gentle slope Plot 3)	SIM, PRO
3	Coarse-sized granoblastic marbles, grain-supported and other massive limestones		medium-high i.e. quartz and clays between 2-5 %	medium-high i.e. t_{60} 1-3 min	very low i.e. t_{60} > 20 min	very high OT (deep slope Plot 3)	IDW
4	Fine-grained marbles and mud-supported limestones		medium-high i.e. quartz and clays between 2-5 %	medium-high i.e. t_{60} 1-3 min	medium-low i.e. t_{60} 4-8 min	low OT (gentle slope Plot 3)	VER, CR1, WOP, SMA

REFERENCES

[1] Obst, K.-H.; Stradtmann, J.; Ullrich, W.; König, G. (1970): Present Status and Technical Advances of Steelworks Lime for Basic Oxygen Furnaces in Germany. The reaction parameters of Lime, ASTM STP, 472, 173-192

[2] Limes, R.W.; Russell, R.O. (1970): Crucible Test for Lime Reactivity in Slags. The Reaction Parameters of Lime, ASTM STP 472, 161-172

[3] Manocha, S.; Ponchon, F. (2018): Management of Lime in Steel. Metals, 8:9, 686, 16 p., https://doi.org/10.3390/met8090686

[4] Boynton, R.S. (1982): Chemistry and Technology of Lime and Limestone. Wiley & Sons, New York, 592 p. ISBN: 978-0-471-02771-3

[5] ASTM C110 (2016): Standard Test Methods for Physical Testing of Quicklime, Hydrated Lime, and Limestone. ASTM Book of Standards, 04.01, 20p

[6] EN 459-2 (2010): Building lime – Part 2: Tests methods. CEN/TC 51, 116p

[7] Eades, J.L.; Sandberg, P.A. (1970): Characterization of the properties of commercial lime by surface area measurements and scanning electron microscopy. ASTM STP, 472, 3-24

[8] McClellan, G.H.; Eades, J.L. (1970): The Textural Evolution of Limestone Calcines. The Reaction Parameters of Lime, ASTM STP, 472, 209-227

[9] Moropoulou, A.; Bakolas, A.; Aggelakopoulou, E. (2001): The effects of limestone characteristics and calcinations temperature to the reactivity of the quicklime. Cem Concr Res, 31, 633-639, https://doi.org/10.1016/S0008-8846(00)00490-7

[10] Hogewoning, S.; Wolter, A., Schmidt, S.-O. (2008): Dependence of hard burn potential on limestone properties. ZKG International, 61:6, 54-60 (Part 1); 61:7, 84-93 (Part 2)

[11] Kiliç, Ö. (2013): Impact of Physical Properties and Chemical Composition of Limestone on Decomposition Activation Energy. Asian Journal of Chemistry, 25:14, 8116-8120, http://www.asianjournalofchemistry.co.in/User/ViewFreeArticle.aspx?ArticleID=25_15_105

[12] Lech, R.; Wodnicka, K.; Pedzich, Z. (2009): Effect of the limestone fabric on the fabric development in burnt lime. ZKG International, 6/7, 62, 94-101 (part 1); 8, 62, 63-72 (part 2)

[13] Rodriguez-Navarro, C.; Ruiz-Agudo, E.; Luque, A.; Navarro, A.B.; Ortega-Huertas, M. (2009): Thermal decomposition of calcite: Mechanisms of formation and textural evolution of CaO nanocrystals. American Mineralogist 94:4, 578-593. https://doi.org/10.2138/am.2009.3021

[14] Soltan, A.M.M. (2009): Petrographic modelling of Egyptian limestones for quicklime manufacture. Arabian Journal of Geosciences, 4, 803–815. https://doi.org/10.1007/s12517-009-0095-4

[15] Soltan A.M.M.; Serry, M.A.-K. (2011): Impact of limestone microstructure on calcination activation energy. Advances in Applied Ceramics, 110:7, 409-416, https://doi.org/10.1179/1743676111Y.0000000042

[16] Alaabed, S.; Soltan, M.A.; Abdelghany, O.; Amin, B.E.M.; Tokhi, M.E.; Khaleel, A.; Musalim, A. (2014): United Arab Emirates limestones: impact of petrography on thermal behaviour. Mineralogy and Petrology, 108:6, 837-852, https://doi.org/10.1007/s00710-014-0329-3

[17] Vola, G.; Sarandrea, L.; Della Porta, G.; Cavallo, A.; Jadoul, F.; Cruciani, G. (2017): The influence of petrography, mineralogy and chemistry on burnability and reactivity of quicklime produced in Twin Shaft Regenerative (TSR) kilns from Neoarchean limestone (Transvaal Supergroup, South Africa). Mineralogy and Petrology, 112:4, 555-576, https://doi.org/10.1007/s00710-017-0542-y

[18] Vola, G.; Bresciani, P.; Rodeghero, E.; Sarandrea, L.; Cruciani, G. (2018): Impact of rock fabric, thermal behavior, and carbonate decomposition kinetics on quicklime industrial production and slaking reactivity. Journal of Thermal Analysis and Calorimetry, 136:3, 967-993, https://doi.org/10.1007/s10973-018-7769-7

[19] Vola, G. (2019): High-grade burnt lime products: impact of calcination kinetics on slaking reactivity; sticking tendency and blocks formation at HT (1300 °C). International PhD Thesis in Earth and Marine Sciences (XXXI cycle), University of Ferrara, Italy, 282 p.

[20] Schorcht, F. ; Kourti, I. ; Scalet, B.M. ; et al. (2013): Best Available Techniques (BAT) Reference Document for the Production of Cement, Lime and Magnesium Oxide. Joint Research Center (JRC), 171-292, http://eippcb.jrc.ec.europa.eu/reference/BREF/CLM_Published_def.pdf

[21] Hai Do, D.; Specht, E.; Kehse, G.; Ferri, V.; Christiansen, T.L.; Bresciani, P. (2011): Simulation of lime calcination in PFR kiln. Influence of energy input and lime throughput. ZKG International, 12, 52-64.

[22] Flügel, E. (2010): Microfacies of Carbonate Rocks. Analysis, interpretation and application. Springer-Verlag Berlin, Heidelberg, 984 p. ISBN: 978-3-642-03795-5

[23] Young, R.A. (ed.) (1993): The Rietveld method. IUCr, Monograph on Crystallography, No. 5, Oxford University Press, 298 p. ISBN 0–19–855577–6

[24] Elsen, J.; Mertens, G.; Snellings, R. (2011): Portland cement and other calcareous hydraulic binders: History, production and mineralogy. In: G.E. Christidis (Ed.) "Advances in the characterization of industrial minerals", EMU Notes in mineralogy, London, 9:1, 441-479, https://doi.org/10.1180/EMU-notes.9.11

[25] Commandré, J.-M.; Salvador, S.; Nzihou, A. (2007): Reactivity of laboratory and industrial limes. Chemical Engineering Research and Design, 85:4, 473-480, https://doi.org/10.1205/cherd06200

[26] Shi, H.; Zhao, Y.; Li, W. (2002); Effects of temperature on the hydration characteristics of free lime, Cement & Concrete Research, 32:5, 789-793, https://doi.org/10.1016/S0008-8846(02)00714-7

[27] Vola, G.; Jadoul, F. (2014); Applied stratigraphy and carbonate petrography of the Arabescato Orobico dimension stone from the Bergamasc Alps (Calcare Rosso, Italy). Italian Journal of Geosciences, 133:2, 294-314, https://doi.org/10.3301/IJG.2014.11